Manufacturing Letters 29 (2021) 74–78

Contents lists available at ScienceDirect

Manufacturing Letters

journal homepage: www.elsevier.com/locate/mfglet

Letters

Surface prediction and measurement for modulated tool path (MTP) turning

Ryan Copenhaver [a], Scott Smith [b], Tony Schmitz [a,b,*]

[a] University of Tennessee, Mechanical, Aerospace, and Biomedical Engineering, Knoxville, TN, USA
[b] Oak Ridge National Laboratory, Manufacturing Science Division, Oak Ridge, TN, USA

ARTICLE INFO

Article history:
Received 22 February 2021
Received in revised form 21 May 2021
Accepted 1 July 2021
Available online 17 July 2021

Keywords:
Turning
Surface finish
Modulated tool path

ABSTRACT

This paper describes a time-domain simulation for predicting surface finish in modulated tool path (MTP) turning, which uses sinusoidal axis motions in the feed direction to produce discontinuous chips for ductile workpiece materials. The simulation includes: the low frequency and low amplitude tool oscillation in the feed direction; the time-varying chip thickness, cutting force, and tool displacement; and the plastic side flow effect used to calibrate the effective tool nose radius. Comparisons between predicted and measured surface profiles are presented for turning a 6061-T6 aluminum cylinder as a function of the MTP oscillation frequency and amplitude with discontinuous chip formation.

1. Introduction

The formation of continuous stringy chips is problematic for many single-point cutting operations such as turning and boring. The long continuous chips can wrap around the tool or workpiece, damage the surface, and require manual intervention for removal. A variety of strategies for ensuring broken chips have been proposed including high pressure coolant and chip breaking geometries. These strategies have had mixed success and there has been substantial prior research activity focused on chip formation mechanisms and chip breakability, including two CIRP keynote papers [1,2]. Zhang and Peklenik [3] discussed chip control in difficult-to-machine materials. Jawahir [4] used high-speed video to examine the mechanisms of chip flow, chip curl, and chip breaking. Fang and Jawahir [5] modeled the chip formation and chip/-work interaction to predict when chips would break. In [6], Andreasen and De Chiffre described the experimental elaboration of chip breaking diagrams for predicting machining parameters that cause chip breaking. Sata *et al.* [7] and Childs *et al.* [8] described the computation of surface finish in turning operations.

More recently, a new modulated tool path (MTP) strategy has been described (see [9,10], for example) that uses modulation of the tool motion in the direction of the feed motion to interrupt the cut, causing the chips to break. Because the axes of the CNC machine tool are used to cause the motion that breaks the chips, no special equipment is required and the NC program for most single-point cutting operations can be modified to ensure chip breaking. Smith [11] discussed the dynamic ability of machine tool axes to execute the MTP strategy. In [12], Smith used the geometry of the cutting edge and the kinematics of the tool motion to estimate the surfaces produced using MTP, for a variety of workpiece geometries, showing that many possible parameter settings produce both broken chips and smooth surfaces. In [13,14], Copenhaver and Schmitz included the cutting dynamics and analyzed the stability of MTP turning.

In this work, we describe a simulation program for predicting the surface characteristics in MTP turning, including not only the geometry of the cutting edge and kinematics of the motion, but also the cutting forces, tool vibration, and the chip plastic side flow effect [15] to predict the surface produced. These predictions are compared to surface finish measurements with good agreement.

2. Modeling

The primary steps of the MTP surface prediction algorithm are: 1) define the nominal tool motion using the MTP parameters; 2) calculate the instantaneous chip thickness; 3) calculate the cutting force components using the chip thickness, chip width (depth of cut), and mechanistic cutting force model; 4) compute the tool displacement by numerical integration of the differential equations of motion; 5) sample the tool displacement at a fixed circumferential location for multiple workpiece revolutions; and 6) superimpose the tool nose radius, which is calibrated by the plastic side flow effect, at these locations to predict the surface finish. The MTP feed motion, z_f, is described by:

* Corresponding author.
E-mail address: tony.schmitz@utk.edu (T. Schmitz).

https://doi.org/10.1016/j.mfglet.2021.07.001

$$z_f = \left(\frac{\Omega}{60} f_r\right) t + RAF \cdot f_r \cdot \sin\left(\frac{\Omega}{60} 2\pi \cdot OPR \cdot t\right) z_f = \left(\frac{\Omega}{60} f_r\right) t + RAF \cdot f_r \cdot \sin\left(\frac{\Omega}{60} 2\pi \cdot OPR \cdot t\right) \quad (1)$$

where f_r is the feed per revolution, *RAF* (Ratio of Amplitude to Feed) is the ratio of the MTP motion amplitude to f_r, Ω is the spindle speed (rpm), and *OPR* (Oscillations Per Revolution) is the number of sinusoidal MTP oscillations per workpiece revolution [12]. An example feed motion is displayed in Fig. 1, where the feed per revolution is 0.1 mm, the spindle speed is 200 rpm, and the *RAF* and *OPR* values are 0.8 and 0.5. The constant feed result is identified by the dashed line, while the solid line shows the MTP motion. The variable tool motion is parsed by revolution using the vertical dotted lines; three revolutions are shown.

The instantaneous chip thickness calculation is shown in Fig. 2. By superimposing the three revolutions from Fig. 1 (the time for one revolution is 0.3 s), the time-dependent chip thickness, h, for revolution 2 (filled area) is determined from the vertical distance (tool motion) between revolutions 1 and 2. Note that the chip thickness is zero for all time that the revolution 2 motion appears below revolution 1, i.e., no tool-workpiece contact occurs. The chip thickness for revolution 3 is the vertical distance between revolution 3 and 2; because revolution 3 always appears above revolution 2, the chip thickness is always greater than zero.

The chip thickness, h, for a rigid tool (and workpiece) is computed by:

$$h = z_{f,n} - \max\{z_{f,n-1}, z_{f,n-2}, \cdots\} \quad (2)$$

where n is the current revolution. The chip thickness is, of course, modified by displacement of the flexible tool. The tool displacement, z_t, in the feed direction is incorporated using Eq. (3), where z_t is considered positive out of the cut as shown in Fig. 3.

$$h = (z_{f,n} - z_{t,n}) - \max\{(z_{f,n-1} - z_{t,n-1}), (z_{f,n-2} - z_{t,n-2}), \cdots\} \quad (3)$$

Given the chip thickness from Eq. (3) and the chip width, b, the cutting force components in the tangential (t), normal (n), and radial (r) directions (Fig. 3) are calculated using:

$$F_t = k_t b h \quad (4)$$

$$F_n = k_n b h \quad (5)$$

$$F_r = k_r b h \quad (6)$$

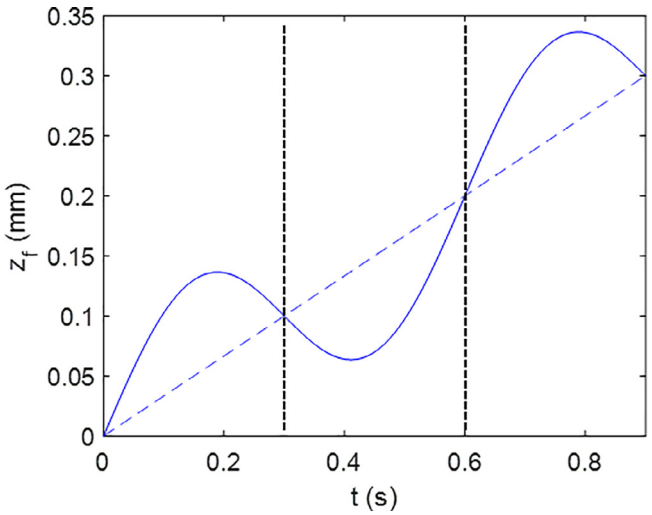

Fig. 1. Example MTP feed motion.

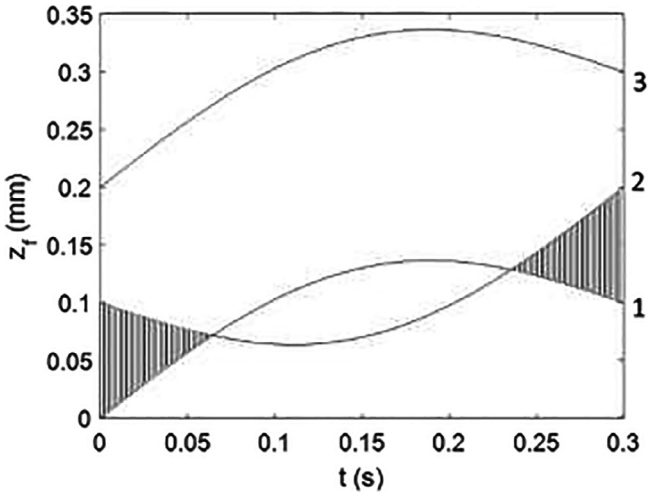

Fig. 2. Chip thickness calculation. The non-zero chip thickness during revolution 2 is identified by the filled areas.

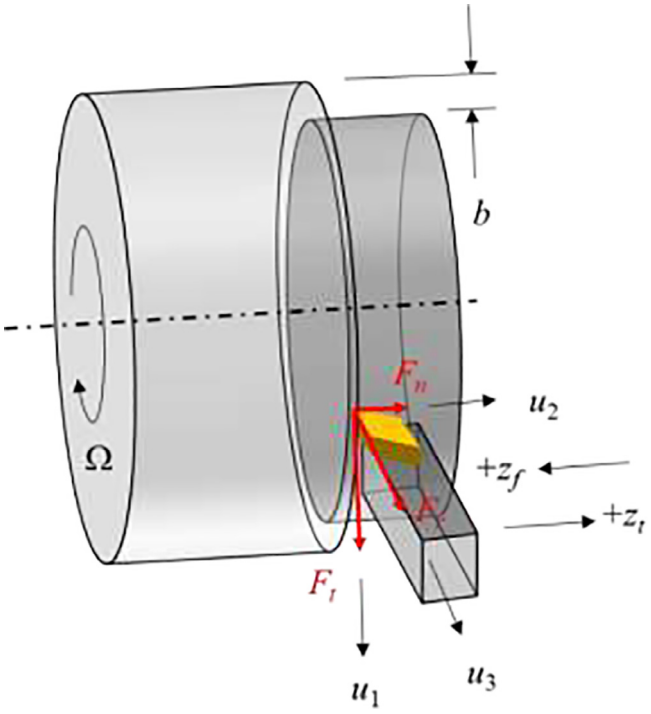

Fig. 3. Schematic of the MTP surface finish model with: MTP feed motion, z_f, and tool displacement, z_t; force components in the tangential, F_t, and normal, F_n, and radial, F_r, directions; directions for the modal parameters, u_1, u_2, and u_3; and the chip width, b, and spindle speed, Ω.

where the cutting force coefficients, $k_{t/n/r}$, are determined by measuring the force using a cutting force dynamometer under constant feed conditions. Semi-implicit Euler integration is then applied to calculate the acceleration, velocity, and displacement, u, in the three modal directions using the appropriate force component and modal parameters. See Eq. (7) for the u_1 direction, which corresponds to the tangential force direction; the equations are similar for the other two directions, but the force component and modal parameters change. The modal mass, m, viscous damping coefficient, c, and stiffness, k, values are obtained by performing impact tests using an instrumented hammer and low mass accelerometer and modal fitting to extract the parameters from the measured frequency

response functions. Multiple vibration modes in each direction are accommodated by summing the individual modal contributions after numerical integration.

$$\begin{aligned} \ddot{u}_1 &= \frac{F_t - c_{u1}\dot{u}_1 - k_{u1}u_1}{m_{u1}} \\ \dot{u}_1 &= \dot{u}_1 + \ddot{u}_1 dt \\ u_1 &= u_1 + \dot{u}_1 dt \end{aligned} \tag{7}$$

To determine the surface finish considering the MTP feed and dynamic displacements, a location around the cylindrical machined surface circumference is first selected. This location represents the position where a line trace would be performed in the z_f direction to determine the local surface profile. Given this location, the corresponding $z_f - z_t$ value is recorded for each revolution; see Fig. 4, where d is the distance in the circumferential direction and four revolutions are shown.

Once the tool feed positions are extracted using Fig. 4, the tool nose radius is then superimposed at those same locations to define the machined surface. The radial displacement, u_3, is used to offset the nose radius in the vertical direction and, therefore, accommodate vibration in the direction normal to the machined surface. Note that the instantaneous b value in Eqs. (4)–(6) is also updated using u_3. Fig. 5 displays the result, where r is the radial direction that defines the machined surface normal. The minimum value is selected at each location along the surface trace (z direction) in the left panel to yield the final MTP surface finish in the right panel. The tool nose radius in Fig. 5 is calibrated using the concept of plastic side flow and data from constant feed turning tests, as described in the following section.

2.1. Experimental validation

The experimental setup is displayed in Fig. 6, which includes a Haas TL-1 CNC lathe, 6061-T6 aluminum workpiece, VMBT-331 (35 deg diamond) carbide insert clamped in a toolholder, and Keyence LK-H157 laser triangulation displacement sensor to measure the feed motion.

As a first step, the cutting force coefficients were determined by measuring the three force components during constant feed tests at feed per revolution values ranging from 0.05 mm to 0.35 mm in 0.05 mm increments. The depth of cut was 0.127 mm and the spindle speed was 1056 rpm (244 m/min cutting speed). The nonlinear coefficients are provided in Eqs. 8–10, where the units are N/mm^2 and the chip thickness is expressed in mm.

$$k_t = 131.1h^{-0.89} + 702.1 \tag{8}$$

$$k_n = 39.1h^{-0.97} + 111.8 \tag{9}$$

$$k_r = 124.1h^{-0.99} + 564.4 \tag{10}$$

The plastic side flow effect calibration is shown in Fig. 7. A constant feed test was conducted at a feed per revolution of 0.051 mm with a 0.127 mm depth of cut and 1056 rpm spindle speed (244 m/min cutting speed). The physical nose radius for the insert was 0.397 mm. The simulation from the previous section was executed with zero *RAF* and *OPR* and the nose radius was modified until the measured and predicted surface profiles agreed. This effective nose radius, which presumably captures plastic side flow effects, was 0.234 mm and was used for all subsequent predictions. Note that Fig. 7 includes the measured profile, predicted profile using the physical nose radius, and the new profile using the effective radius obtained from the single calibration test.

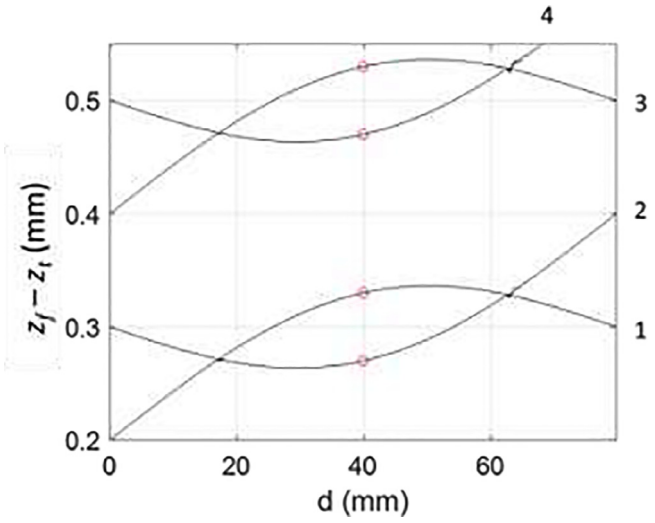

Fig. 4. MTP tool feed position for four spindle revolutions. A single circumferential location is identified by a circle for all four revolutions.

3. Results

Simulations and experiments were completed for: 1) *OPR* values from 0.2 to 0.8 with a fixed *RAF* value of 0.8; and 2) *RAF* values from 0.5 to 1.1 with a fixed *OPR* value of 0.5. The depth of cut was 0.127 mm and the spindle speed was 1056 rpm for each test; all MTP parameter combinations yielded discontinuous chips. Fig. 8 shows results for (top) *OPR* = 0.3 and (bottom) *OPR* = 0.5 with *RAF* = 0.8 in each case. Good agreement is observed, even though the surface profiles are quite different. Measurements were performed using a Mitutoyo Contracer stylus profilometer. To summarize the predicted and measured surface profiles, the average roughness, Ra, was calculated for each test condition. Fig. 9 shows the results for varying (top) *OPR* and (bottom) *RAF*. It is seen that the Ra values are mirrored about an *OPR* value of 0.5 and decrease for increasing *RAF* values up to 1.

An important contribution of this paper is the inclusion of the side flow effect for nose radius calibration. The addition of side flow has been previously reported to improve the accuracy of surface finish predictions for turning [15]. The approach in [15] was to modify the Ra equation by adding a new term. In reference [12], the authors use only the cutting edge and kinematic MTP tool motion to predict surface finish and the predictions do not generally agree with experiments. The study presented here is the first to demonstrate an approach that is able to accurately predict surface profiles and surface roughness for MTP turning operations over a wide range of MTP parameters.

Future work will focus on the proposed side flow effect. Additional research is required to determine if the proper description for the difference between the calibrated and actual nose radius is, in fact, "plastic side flow". Practically speaking, Figs. 8 and 9 demonstrate that accurate prediction of MTP surface profiles is possible using a single calibrated nose radius. Follow-on testing is warranted to compare best-fit nose radii for different feed per revolution values, surface speeds, tool geometries, and work materials.

4. Conclusions

This paper describes a time-domain simulation program for predicting surface finish profiles in modulated tool path (MTP) turning. The simulation includes: the MTP tool motion; the time-varying chip thickness, cutting force components, and tool dis-

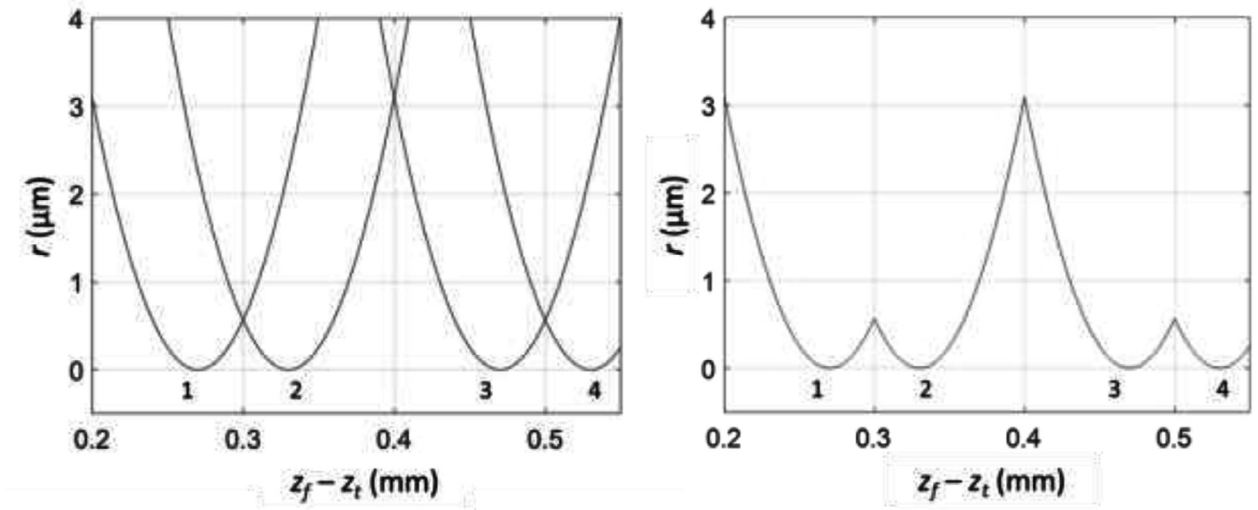

Fig. 5. (Left) Tool nose radius superimposed on the MTP tool position for four spindle revolutions. (Right) MTP surface finish prediction for four spindle revolutions.

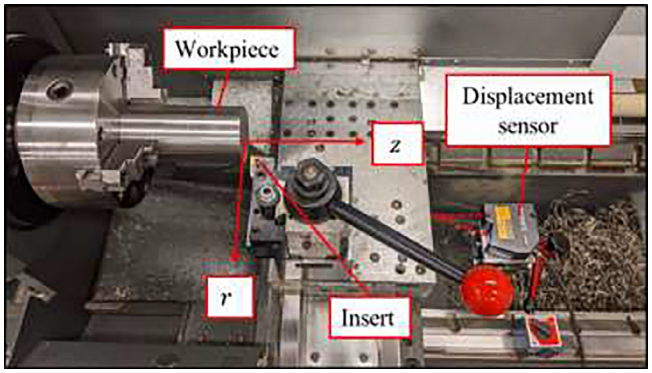

Fig. 6. Turning setup.

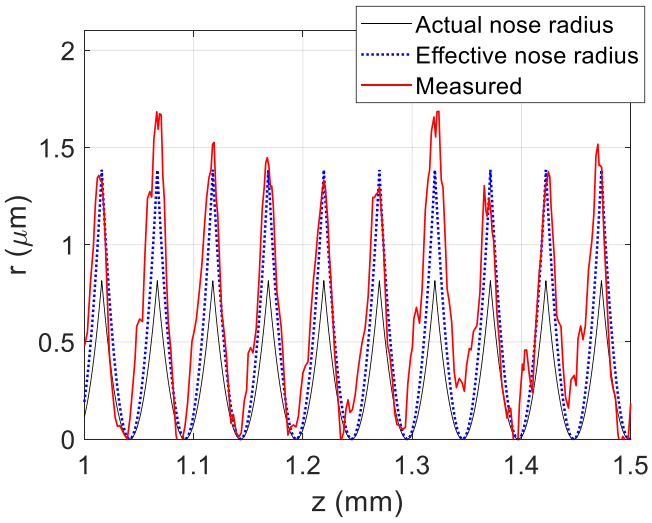

Fig. 7. Plastic side flow effect nose radius calibration.

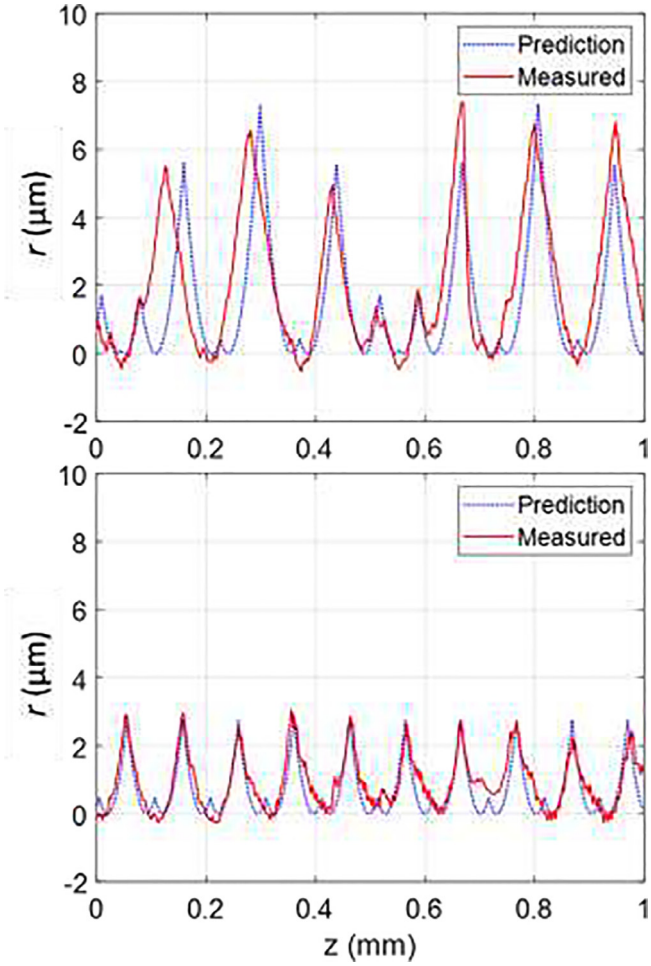

Fig. 8. Predicted and measured surface profiles for *RAF* = 0.8 with (top) *OPR* = 0.3 and (bottom) *OPR* = 0.5.

placements; and surface profile prediction using an effective tool nose radius, which incorporates the plastic side flow effect. Results were presented which demonstrated good agreement between predicted and measured surface profiles. Average roughness trends were plotted as a function of MTP parameters describing the feed direction oscillation frequency and amplitude. Prediction and experiment show good agreement.

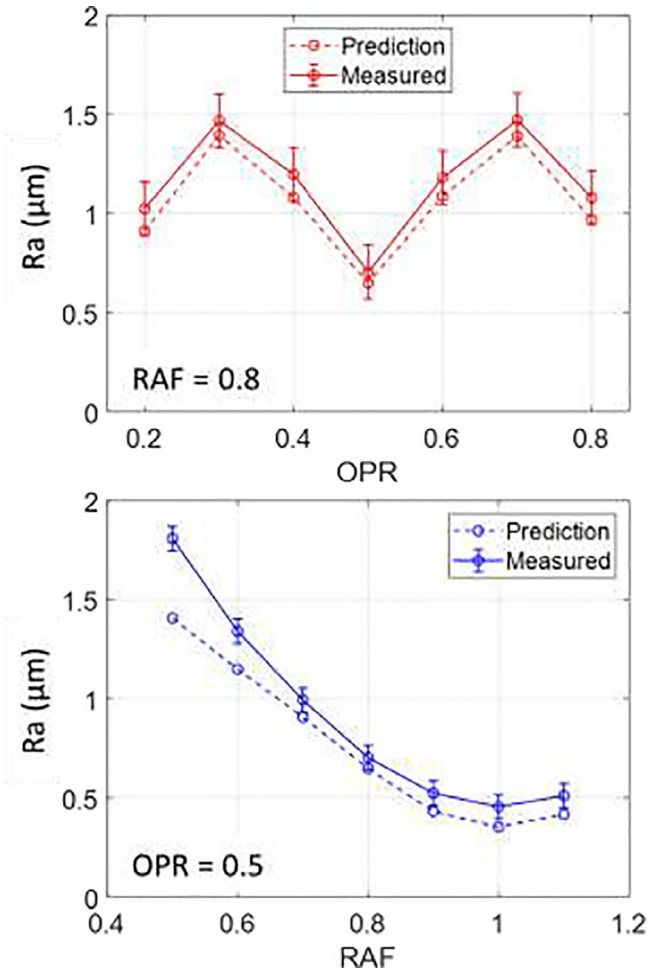

Fig. 9. Predicted and measured Ra as a function of (top) *OPR* and (bottom) *RAF*. The error bars represent +/− one standard deviation from three measurements at different circumferential locations.

Declaration of Competing Interest

The authors declare that they have no known competing financial interests or personal relationships that could have appeared to influence the work reported in this paper.

Acknowledgements

This research was supported by Consolidated Nuclear Security, LLC and the DOE Office of Energy Efficiency and Renewable Energy (EERE), Manufacturing Science Division, and used resources at the Manufacturing Demonstration Facility, a DOE-EERE User Facility at Oak Ridge National Laboratory.

References

[1] Kluft W et al. Present knowledge of chip control. Ann CIRP 1979;28(2):441–55.
[2] Tönshoff HK, Wulfsberg JP, Kals HJJ, König W, van Luttervelt CA. Developments and trends in monitoring and control of machining processes. Ann CIRP 1988;37(2):611–22.
[3] Zhang YZ, Peklenik J. Chip curl, chip breaking and chip control of the difficult-to-cut materials. Ann CIRP 1980;29(1):79–83.
[4] Jawahir IS. On the controllability of chip breaking cycles and modes of chip breaking in metal machining. Ann CIRP 1990;39(1):47–51.
[5] Fang XD, Jawahir IS. An analytical model for cyclic chip formation in 2-D machining with chip breaking. Ann CIRP 1996;45(1):53–8.
[6] Andreasen JL, De Chiffre L. An automatic system for elaboration of chip breaking diagrams. Ann CIRP 1998;47(1):35–40.
[7] Sata T, Li M, Takata S, Hiraoka H, Li CQ, Xing XZ, et al. Analysis of surface roughness generation in turning operation and its applications. Ann CIRP 1985;34(1):473–6.
[8] Childs THC, Sekiya K, Tezuka R, Yamane Y, Dornfeld D, Lee D-E, et al. Surface finishes from turning and facing with round nosed tools. Ann CIRP 2008;57(1):89–92.
[9] Woody BA et al. Chip breaking in turning operations in CNC toolpaths. Trans NAMRI 2008;36:1–8.
[10] Woody BA et al. Assessment of the process parameters and their effect on the chip length when using CNC toolpaths to provide chip breaking in turning operations. In: Proceedings of the 3rd ASME MSEC Conference. p. 533–40. https://doi.org/10.1115/MSEC_ICMP2008-72468.
[11] Smith S, Woody B, Barkman W, Tursky D. Temperature control and machine dynamics in chip breaking using CNC toolpaths. Ann CIRP 2009;58(1):97–100.
[12] Smith S, McFarland J, Assaid T, Tursky D, Barkman W, Babelay E. Surface characteristics generated in CNC chip breaking tool paths. Ann CIRP 2010;59(1):137–40.
[13] Copenhaver R, Schmitz T, Smith S. Stability analysis of modulated tool path turning. Ann CIRP 2018;67(1):49–52.
[14] Copenhaver R, Schmitz T. Modeling and simulation of modulated tool path (MTP) turning stability. Manuf Lett 2020;24:67–71.
[15] Liu K, Melkote SN. Effect of plastic side flow on surface roughness in micro-turning process. Int J Mach Tools Manuf 2006;46(14):1778–85.